Volume 1 | Number 1 | Jan 2013 | Pages 1–100

Polymer Chemistry

www.rsc.org/polymers

ROYAL SOCIETY OF CHEMISTRY

ROYAL SOCIETY OF CHEMISTRY

www.rsc.org/polymers

Table of Contents for:

Doubly thermo-responsive ABC triblock copolymer nanoparticles prepared through dispersion RAFT polymerization

Quanlong Li, Chengqiang Gao, Shentong Li, Fei Huo, and Wangqing Zhang*

Key Laboratory of Functional Polymer Materials of the Ministry of Education, Collaborative Innovation Center of Chemical Science and Engineering (Tianjin), Institute of Polymer Chemistry, Nankai University, Tianjin 300071, China.
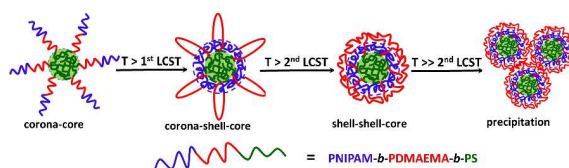
Doubly thermo-responsive triblock copolymer nanoparticles are prepared by dispersion RAFT polymerization and the nanoparticles exhibit two-step phase-transition with temperature increasing.

Journal Name

ARTICLE

Doubly thermo-responsive ABC triblock copolymer nanoparticles prepared through dispersion RAFT polymerization

Quanlong Li, Chengqiang Gao, Shentong Li, Fei Huo, and Wangqing Zhang*

Doubly thermo-responsive triblock copolymer nanoparticles of poly(*N*-isopropylacrylamide)-*block*-poly[*N,N*-(dimethylamino) ethyl methacrylate]-*block*-polystyrene (PNIPAM-*b*-PDMAEMA-*b*-PS) and PDMAEMA-*b*-PNIPAM-*b*-PS containing two thermo-responsive blocks of poly(*N*-isopropylacrylamide) (PNIPAM) and poly[*N,N*-(dimethylamino) ethyl methacrylate] (PDMAEMA) are prepared by macro-RAFT agent mediated dispersion polymerization through polymerization-induced self-assembly. The RAFT polymerization undergoes an initial slow homogeneous polymerization and then a fast heterogeneous one. During the dispersion RAFT polymerization, the molecular weight of the synthesized triblock copolymer linearly increases with the monomer conversion and the average diameter of the in situ synthesized triblock copolymer nanoparticles increases with the triblock copolymer molecular weight. The triblock copolymer nanoparticles exhibit two separate lower critical solution temperatures (LCST) corresponding to the PNIPAM block and the PDMAEMA block in water, and this two-step thermo-responsive behavior is evidenced by the combined techniques including turbidity analysis, variable temperature ^{1}H NMR analysis, DLS analysis and TEM observation. It is found that the first LCST corresponding to the PNIPAM block and the second LCST corresponding to the PDMAEMA block tethered on the polystyrene core of the triblock copolymer nanoparticles are much higher than those of the reference homopolymers, and the reason is ascribed to the steric repulsion and the strong interaction between the PNIPAM and PDMAEMA blocks. Besides, the difference in the thermo-responsive behavior of the triblock copolymer nanoparticles of PNIPAM-*b*-PDMAEMA-*b*-PS and PDMAEMA-*b*-PNIPAM-*b*-PS ascribed to the different block order is demonstrated.

1 Introduction

Over the past decade, block copolymer nano-objects, especially thermo-responsive block copolymer nano-objects, have aroused great interest because of their potential use in drug delivery, electronics, and catalysis.[1-2] Usually, two types of thermo-responsive polymers are clarified. The first is the thermo-responsive polymer exhibiting the lower critical solution temperature (LCST) in solvent,[3-14] in which poly(*N*-isopropylacrylamide) (PNIPAM) possessing LCST around 32 ºC in water gains the most focused attention.[8-12] This LCST-type thermo-responsive polymer is molecularly soluble in solvent at temperature below LCST. When temperature increases above LCST, the soluble-to-insoluble phase transition occurs and the polymer becomes insoluble. The second is the thermo-responsive polymer showing insoluble-to-soluble phase transition at the upper critical solution temperature (UCST),[15-19] in which the thermo-responsive behavior is just different from that of the LCST-type one. When two or more than two thermo-

responsive polymeric segments are included in a single polymer chain, multi-thermo-responsive copolymers showing multiple LCSTs, UCSTs or one segment presenting LCST whereas the other presenting UCST are obtained.[20-28] Recently, benefiting from the controlled radical polymerization (CRP) techniques such as atom transfer radical polymerization (ATRP)[29-31], nitroxide-mediated polymerization (NMP)[32] and reversible addition-fragmentation chain transfer (RAFT) polymerization[33-37], various multiply thermo-responsive block copolymers such as poly(propylene oxide)-*block*-poly(2-methacryloyloxyethyl phosphorylcholine)-*block*-poly(*N*-isopropylacrylamide),[20] poly[oligo(ethylene glycol) monomethyl ether methacrylate]-*block*-poly(*N*-isopropyl methacrylamide),[21] poly[2-(dimethylamino)ethyl methacrylate]-*block*-poly[di(ethyleneglycol) methyl ether methacrylate],[24] poly[2-(2-methoxyethoxy)ethyl methacrylate]-*block*-poly[*N*-(4-vinylbenzyl)-*N,N*-diethylamine][27] and poly[*N*-(4-vinylbenzyl)-*N,N*-dimethylamine]-*block*-poly[*N*-(4-vinylbenzyl)-*N,N*-diethylamine]-*block*-poly[*N*-(4-vinylbenzyl)-*N,N*-

dimethylamine],[28] have been synthesized. Compared with the general thermo-responsive block copolymers containing a single thermo-responsive block,[8-17] these multi-thermo-responsive block copolymers contain two or more thermo-responsive blocks and therefore much more complex phase behaviour is demonstrated. In fact, various multi-thermo-responsive block copolymer nano-objects have been fabricated through the micellization strategy, and the size or even the morphology of the multi-thermo-responsive block copolymer nano-objects can be tuned by increasing/decreasing the temperature above/below LCST of the thermo-responsive blocks.[23-28]

Recently, polymerization-induced self-assembly (PISA) has been demonstrated to be a convenient method to prepare block copolymer nano-objects.[38,39] Following this PISA strategy, the macro-RAFT agent mediated emulsion polymerization or dispersion polymerization is performed and one-pot synthesis of highly concentrated block copolymer nano-objects is achieved.[40-59] Compared with the micellization strategy, the PISA method has three advantages including (1) concentrated block copolymer nano-objects (10~30 wt%), (2) the relative simple usually one-pot polymerization to implement, and (3) the tunable structure of the block copolymer nano-objects. However, seldom effort has been made to prepare thermo-responsive block copolymer nano-objects through the PISA strategy under dispersion conditions, although several examples of PNIPAM-based block copolymer nano-objects have been reported.[45,59,60]

In this contribution, two kinds of doubly thermo-responsive ABC triblock copolymer nanoparticles of poly(*N*-isopropylacrylamide)-*block*-poly[*N,N*-(dimethylamino) ethyl methacrylate]-*block*-polystyrene (PNIPAM-*b*-PDMAEMA-*b*-PS) and poly[*N,N*-(dimethylamino) ethyl methacrylate]-*block*-poly(*N*-isopropylacrylamide)-*block*-polystyrene (PDMAEMA-*b*-PNIPAM-*b*-PS), in which the PNIPAM block exhibits the first LCST and the PDMAEMA block shows the second LCST in water, were prepared by dispersion RAFT polymerization in the 80/20 methanol/water mixture (by weight). After transferring these triblock copolymer nanoparticles from the 80/20 methanol/water mixture into neat water, the doubly thermo-responsive behavior of these triblock copolymer nanoparticles dispersed in water is checked and the different thermo-response between the PNIPAM-*b*-PDMAEMA-*b*-PS and PDMAEMA-*b*-PNIPAM-*b*-PS nanoparticles is demonstrated. It is found that, these PNIPAM-*b*-PDMAEMA-*b*-PS corona-core nanoparticles dispersed in water initially convert into corona-shell-core nanoparticles at temperature above the first LCST of the PNIPAM block. With temperature increasing above the second LCST of the poly[*N,N*-(dimethylamino) ethyl methacrylate] (PDMAEMA) block, these corona-shell-core nanoparticles can further converts into shell-shell-core ones.

2 Experimental

2.1 Materials

The monomer of *N*-isopropylacrylamide (NIPAM, >99%, Acros Organics) was purified by recrystallization in the acetone/*n*-hexane mixture (50:50 by volume). The monomer of *N,N*-(dimethylamino) ethyl methacrylate (DMAEMA, 98%, Alfa, Scheme 1) was dried with CaH_2 overnight and distilled under reduced pressure prior to use. Styrene (St, >98%, Tianjin Chemical Company) was distilled under vacuum and stored at -5 °C prior to use. 2,2'-Azobis(2-methylpropionitrile) (AIBN, >99%, Tianjin Chemical Company) was recrystallized from ethanol before being used. The RAFT agent of 4-cyano-4-(dodecylsulfanylthiocarbonyl) sulfanyl pentanoic acid (CDTPA, Scheme 1) was synthesized as discussed elsewhere.[61] Other chemical reagents were analytic grade and were used as received. Deionized water was used in the present experiments.
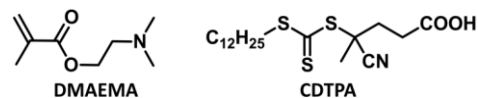
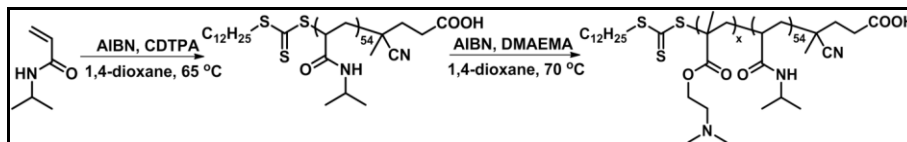**Scheme 1.** The chemical structure of DMAEMA and CDTPA.

2.2 Synthesis of the PNIPAM-*b*-PDMAEMA-TTC macro-RAFT agent

The PNIPAM-*b*-PDMAEMA-TTC macro-RAFT agent was synthesized by sequential solution RAFT polymerization. Herein, the synthesis of the PNIPAM$_{54}$-*b*-PDMAEMA$_{27}$-TTC macro-RAFT agent, in which the subscripts represent the polymerization degree (DP) of the corresponding monomers and TTC represents the RAFT terminal of trithiocarbonate, is typically introduced. Into a 50 mL Schlenk flask with a magnetic bar, NIPAM (8.00 g, 70.7 mmol), CDTPA (322.9 mg, 0.80 mmol), AIBN (32.8 mg, 0.20 mmol) and 1,4-dioxane (30.0 g) were added. The solution was degassed with nitrogen at 0 °C for 30 min, and then the flask content was immersed into a preheated oil bath at 65 °C for 150 min. The polymerization was quenched by rapid cooling upon immersion of the flask in iced water. The monomer conversion of 91% was determined by ^{1}H NMR analysis. The synthesized PNIPAM$_{54}$-TTC was purified by three precipitation/filtration cycles in iced diethyl ether, and then dried under vacuum at room temperature overnight to afford yellow powder (7.0 g, 87% yield). Subsequently, into a 25 mL Schlenk flask with a magnetic bar, DMAEMA (3.72 g, 23.7 mmol), PNIPAM$_{54}$-TTC (3.50 g, 0.54 mmol), AIBN (9.54 mg, 0.058 mmol), the internal standard of 1,3,5-trioxane (0.213 g, 2.33 mmol), and 1,4-dioxane (7.2 g) were added. The solution was degassed with nitrogen at 0 °C for 30 min, and then the flask content was immersed into a preheated oil bath at 70 °C for 4 h. The polymerization was quenched by rapid cooling upon immersion of the flask in iced water. The monomer conversion of 72% was determined by ^{1}H NMR analysis. The synthesized diblock copolymer of PNIPAM$_{54}$-*b*-PDMAEMA$_{27}$-TTC was purified by three precipitation/filtration cycles in *n*-hexane at 0 °C, and then dried under vacuum at room temperature overnight to afford yellow powder (5.2 g, 72% yield).

Table 1. Summary of the PNIPAM-*b*-PDMAEMA-TTC macro-RAFT agents

No.	Macro-RAFT agent	$M_{n,th}$[a] (kg/mol)	$M_{n,NMR}$[b] (kg/mol)	$M_{n,GPC}$[c] (kg/mol)	PDI[d] (M_w/M_n)
1	PNIPAM$_{54}$-TTC	7.2	6.5	5.8	1.10
2	PNIPAM$_{54}$-*b*-PDMAEMA$_{27}$-TTC	12.9	10.7	5.9	1.09
3	PNIPAM$_{54}$-*b*-PDMAEMA$_{46}$-TTC	14.6	13.7	6.3	1.08
4	PNIPAM$_{54}$-*b*-PDMAEMA$_{58}$-TTC	17.0	15.6	6.4	1.09

[a] The theoretical molecular weight determined by monomer conversion. [b] The molecular weight by ^{1}H NMR analysis. [c] The number-average molecular weight by GPC analysis. [d] The PDI or the M_w/M_n values determined by GPC analysis.

Scheme 2. Synthesis of PNIPAM-TTC and PNIPAM-*b*-PDMAEMA-TTC.

2.3 Synthesis of the PDMAEMA-*b*-PNIPAM-TTC macro-RAFT agent

The PDMAEMA$_{30}$-*b*-PNIPAM$_{68}$-TTC or PDMAEMA$_{30}$-*b*-PNIPAM$_{106}$-TTC macro-RAFT agent was prepared by sequential solution RAFT polymerization similarly with the PNIPAM-*b*-PDMAEMA-TTC macro-RAFT agent. Detailed procedures can be found in Supporting Information.

2.4 Dispersion RAFT polymerization of styrene in the methanol/water mixture

The PNIPAM-*b*-PDMAEMA-TTC or PDMAEMA-*b*-PNIPAM-TTC mediated dispersion RAFT polymerization of styrene was performed in the 80/20 methanol/water mixture at 70 ^{o}C under [St]$_0$:[Macro-RAFT]$_0$:[AIBN]$_0$ = 900:3:1 with a constant weight ratio of the feeding styrene monomer to the solvent at 15%. Typically, the diblock copolymer macro-RAFT agent of PNIPAM$_{54}$-*b*-PDMAEMA$_{27}$-TTC (0.161 g, 0.015 mmol), St (0.468 g, 4.5 mmol), AIBN (0.821 mg, 0.0050 mmol) dissolved in the 80/20 methanol/water mixture (3.25 g) were added into a 25 mL Schlenk flask with a magnetic bar. The solution was degassed with nitrogen at 0 ^{o}C for 30 min, and then the polymerization was performed at 70 ^{o}C under vigorous stirring. After a given time, the polymerization was quenched by rapid cooling upon immersion of the flask in iced water. The monomer conversion was detected by UV-vis analysis at 245 nm as discussed elsewhere.[59] The morphology of the in situ synthesized triblock copolymer nano-objects of PNIPAM-*b*-PDMAEMA-*b*-PS was checked with transmission electron microscope (TEM). The synthesized triblock copolymer nano-objects were centrifuged (12500 r/min, 30 min), washed with methanol (20 mL × 3), and dried at 50 °C under vacuum for 24 h for further gel permeation chromatography (GPC) analysis and ^{1}H NMR analysis.

2.5 Characterizations

The GPC analysis was performed on a Waters 600E GPC system equipped with the TSK-GEL columns and a Waters

2414 refractive index detector, where THF containing 3 wt% triethylamine was used as eluent at flow rate of 0.5 mL/min at 30.0 ^{o}C and the narrow-polydispersity polystyrene (molecular weight: 580~280500 Da) was used as calibration standard. The ^{1}H NMR analysis was performed on a Bruker Avance III 400 MHz NMR spectrometer. For polymers dissolved in CDCl$_3$, the proton signal at δ = 7.26 ppm of the internal solvent was used as standard; and for polymers dissolved in D$_2$O, the chemical shift of the internal standard ethanol was locked at δ = 3.37 ppm and was used as reference. The styrene monomer conversion in the RAFT polymerization was determined by UV-vis analysis, in which a given volume of the colloidal dispersion (1.0 mL) was filtrated twice with a 0.22 μm nylon filter, diluted with ethanol, and analyzed by UV-vis analysis. The TEM observation was performed using a Tecnai G^2 F20 electron microscope at an acceleration of 200 kV, whereby a small drop of the dispersion of the triblock copolymer nanoparticles was deposited onto a piece of copper grid, dried at room temperature under vacuum, and then observed by TEM. The LCST of the thermo-responsive polymers was determined by turbidity measurement at 500 nm on a Varian 100 UV-vis spectrophotometer equipped with a thermo-regulator (± 0.1 ^{o}C) with the heating rate at 1 ^{o}C/min. The LCST values were determined at the middle point of the transmittance change. Dynamic light scattering (DLS) analysis was performed on a Nano-ZS90 (Malvern) laser light scattering spectrometer with He-Ne laser at the wavelength of 633 nm at 90° angle, in which the hydrodynamic diameter was determined by intensity following the CONTIN method. The differential scanning calorimetric (DSC) analysis was performed on a NETZSCH DSC calorimeter under nitrogen atmosphere, in which the sample was heated to 140 °C at the rate of 10 °C/min, cooled to 0 °C at 10 °C/min, and then heated to 140 °C at 10 °C/min.

3 Results and discussion

3.1 Synthesis of the PNIPAM-*b*-PDMAEMA-TTC macro-RAFT agent

Table 2. Summary of the PDMAEMA-*b*-PNIPAM-TTC macro-RAFT agents.

| No.	Macro-RAFT agent	$M_{n,th}$ [a] (kg/mol)	$M_{n,NMR}$ [b] (kg/mol)	$M_{n,GPC}$ [c] (kg/mol)	PDI [d] (M_w/M_n)
1	PDMAEMA$_{30}$-TTC	5.9	5.1	3.1	1.23
2	PDMAEMA$_{30}$-*b*-PNIPAM$_{68}$-TTC	15.2	12.8	8.4	1.09
3	PDMAEMA$_{30}$-*b*-PNIPAM$_{106}$-TTC	21.7	17.1	15.2	1.13

[a] The theoretical molecular weight determined by monomer conversion. [b] The molecular weight by ^{1}H NMR analysis. [c] The number-average molecular weight by GPC analysis. [d] The PDI or the M_w/M_n values determined by GPC analysis.

Scheme 2 outlines the synthesis of the diblock copolymer macro-RAFT agent of PNIPAM-*b*-PDMAEMA-TTC, in which the initial synthesis of PNIPAM-TTC by the solution RAFT polymerization of NIPAM initiated by AIBN under $[NIPAM]_0:[CDTPA]_0:[AIBN]_0 = 280:4:1$ and the subsequent synthesis of PNIPAM-*b*-PDMAEMA-TTC by solution RAFT polymerization of DMAEMA in the presence of PNIPAM-TTC under $[DMAEMA]_0:[PNIPAM-TTC]_0:[AIBN]_0 = 360:8:1$ are included. The solution RAFT polymerization of NIPAM runs smoothly, and 91% monomer conversion is achieved in 150 min. The synthesized PNIPAM-TTC is characterized by GPC analysis (Figure 1A) and ^{1}H NMR analysis (Figure 2A). The molecular weight $M_{n,GPC}$ of PNIPAM-TTC by GPC analysis is 5.8 kg/mol, and the low PDI of 1.10 is satisfied. Based on the proton resonance signals at $\delta = 0.88$ ppm corresponding to the RAFT agent terminal and $\delta = 4.00$ ppm corresponding to the polymer main chains shown in Figure 2A, the molecular weight $M_{n,NMR}$ at 6.5 kg/mol and the DP at 54 of the synthesized PNIPAM-TTC are calculated following eq S1 (Seeing in Supporting Information). It is found that the theoretical molecular weight $M_{n,th}$ of PNIPAM-TTC, 7.2 kg/mol, which is calculated by the monomer conversion following eq 1 as described elsewhere,[62] is close to $M_{n,NMR}$ by ^{1}H NMR analysis. However, $M_{n,GPC}$ of the synthesized PNIPAM-TTC by GPC analysis is lower than $M_{n,NMR}$, and the reason is possibly due to the adsorption of the nitrogen-containing polymer of PNIPAM-TTC onto the GPC columns and the unpolar polystyrene standard employed in the GPC analysis, although triethylamine was added in the THF eluent as discussed elsewhere.[63] In the next discussion, the synthesized PNIPAM-TTC is labeled as PNIPAM$_{54}$-TTC, in which the DP at 54 is calculated by $M_{n,NMR}$ determined by NMR analysis.

The PNIPAM-*b*-PDMAEMA-TTC macro-RAFT agent was synthesized by the RAFT polymerization of DMAEMA in 1,4-dioxane using the above synthesized PNIPAM-TTC as macro-RAFT agent and AIBN as initiator. By varying the weight ratio of the feeding DMAEMA/PNIPAM$_{54}$-TTC at 1.06/1, 1.86/1 and 2.66/1, three macro-RAFT agents of PNIPAM$_{54}$-*b*-PDMAEMA$_{27}$-TTC, PNIPAM$_{54}$-*b*-PDMAEMA$_{46}$-TTC and PNIPAM$_{54}$-*b*-PDMAEMA$_{58}$-TTC are prepared. These three PNIPAM-*b*-PDMAEMA-TTC macro-RAFT agents are characterized by GPC analysis (Figure 1) and ^{1}H NMR analysis (Figure 2), and the results are summarized in Table 1. Herein, $M_{n,NMR}$ of the diblock copolymer macro-RAFT agent is calculated by comparing the proton resonance signals at $\delta =$

2.56 ~ 2.80 ppm and 3.88 ~ 4.22 ppm according to eq S2 (Seeing in Supporting Information). As shown in Table 1, the PDI values of the PNIPAM-*b*-PDMAEMA-TTC macro-RAFT agents are below 1.10, and the molecular weight $M_{n,NMR}$ of the diblock copolymer macro-RAFT agents by ^{1}H NMR analysis is close to $M_{n,GPC}$ by GPC analysis. Whereas, the molecular weight $M_{n,GPC}$ by GPC analysis is smaller than $M_{n,NMR}$ by ^{1}H NMR analysis. The underestimated $M_{n,GPC}$ of PNIPAM-*b*-PDMAEMA-TTC is ascribed to the interaction between the tertiary amine groups in the PDMAEMA block and the GPC columns, which leads to the long elution time and therefore the underestimated molecular weight of the diblock copolymer macro-RAFT agent. Besides, the GPC analysis is based on the calibration with the unpolar polystyrene standards, which also contributes the underestimation in the molecular weight of the polar PNIPAM-*b*-PDMAEMA-TTC diblock copolymer.

$$M_{n,th} = \frac{[monomer]_0 \times M_{monomer}}{[RAFT]_0} \times conversion + M_{RAFT} \quad (1)$$
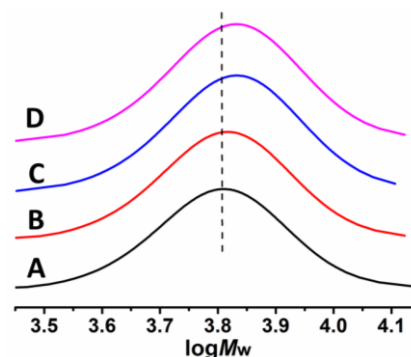
Figure 1. The GPC traces of PNIPAM$_{54}$-TTC (A), PNIPAM$_{54}$-*b*-PDMAEMA$_{27}$-TTC (B), PNIPAM$_{54}$-*b*-PDMAEMA$_{46}$-TTC (C), and PNIPAM$_{54}$-*b*-PDMAEMA$_{58}$-TTC (D).

3.2 Synthesis of the PDMAEMA-*b*-PNIPAM-TTC macro-RAFT agent

Two PDMAEMA-*b*-PNIPAM-TTC macro-RAFT agents, PDMAEMA$_{30}$-*b*-PNIPAM$_{68}$-TTC and PDMAEMA$_{30}$-*b*-PNIPAM$_{106}$-TTC, are also prepared by sequential RAFT polymerization as similar as those of PNIPAM-*b*-PDMAEMA-TTC except in the different polymerization order. The detailed polymerization can be found in Supporting Information. These PDMAEMA-*b*-PNIPAM-TTC macro-RAFT agents are characterized by ^{1}H NMR analysis (Figure S1) and GPC analysis (Figure S2), and the results are summarized in Table 2.
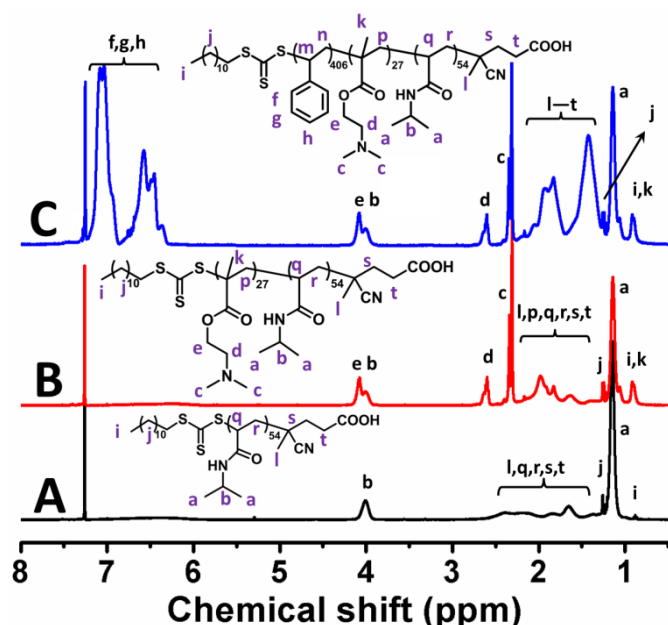
Figure 2. The ^1H NMR spectra of PNIPAM$_{54}$-TTC (A), PNIPAM$_{54}$-*b*-PDMAEMA$_{27}$-TTC (B), and PNIPAM$_{54}$-*b*-PDMAEMA$_{27}$-*b*-PS$_{406}$ (C).
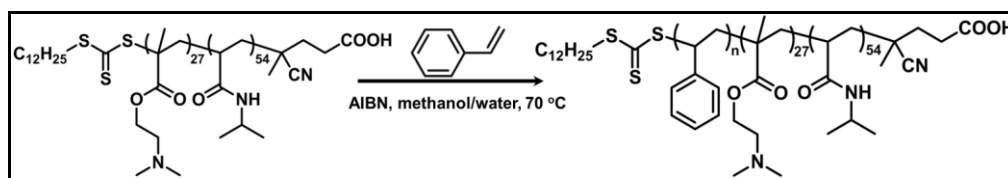
3.3 Dispersion RAFT polymerization of styrene in the methanol/water mixture

The PNIPAM-*b*-PDMAEMA-TTC macro-RAFT agent mediated dispersion RAFT polymerization of styrene was performed in the 80/20 methanol/water mixture as shown in Scheme 3. The solvent of the 80/20 methanol/water mixture is chosen because it is a good solvent of the St monomer and the PNIPAM-*b*-PDMAEMA-TTC macro-RAFT agent but a nonsolvent of the PS block, which is essential for the polymerization-induced self-assembly to prepare the PNIPAM-*b*-PDMAEMA-*b*-PS triblock copolymer nanoparticles.

It is optically observed that the dispersion RAFT polymerization undergoes an initial homogeneous stage and a subsequent heterogeneous stage as similar as the other linear macro-RAFT agent mediated dispersion RAFT polymerizations reported by Armes and by our research group.[48-59] This two-stage polymerization is due to the PNIPAM-*b*-PDMAEMA-*b*-PS triblock copolymer synthesized in the initial stage being molecularly soluble in the polymerization medium at the polymerization temperature and it becoming insoluble with the extension of the solvophobic PS block in the later polymerization. Figure 3A shows the monomer conversion *vs* polymerization time plots for the typical PNIPAM$_{54}$-*b*-

PDMAEMA$_{27}$-TTC macro-RAFT agent mediated dispersion RAFT polymerization, in which a slow monomer conversion in the initial 2 h and a subsequent fast monomer conversion in the next 4 h are observed, and almost complete monomer conversion is achieved when polymerization extends to 10 h. Figure 3B shows the ln([M]$_0$/[M]) *vs* polymerization time plot, in which a two-stage plot containing a gradient linear stage corresponding to the initial homogeneous polymerization and a steep linear one corresponding to the later heterogeneous polymerization is observed. The apparent polymerization rate constants (K_p^{app}),[64] which are calculated by the slope of the ln([M]$_0$/[M]) *vs* the polymerization time plot in the linear part in the homogeneous and heterogeneous polymerization stages, are 0.10 and 0.34 h^{-1}, confirming the heterogeneous polymerization running faster than the homogeneous one. The reason that the RAFT polymerization under heterogeneous condition runs faster than those under homogeneous condition is well clarified, and the radical segregation or the compartmentalization effect under heterogeneous condition is ascribed.[65] Figure 3C shows the GPC traces of the synthesized PNIPAM$_{54}$-*b*-PDMAEMA$_{27}$-*b*-PS triblock copolymers, from which the unimodal GPC traces and the clear shift from low molecular weight to high one with the monomer conversion are observed, indicating the extension of the PS block during the dispersion RAFT polymerization. The molecular weight $M_{n,GPC}$ and PDI of the synthesized PNIPAM-*b*-PDMAEMA-*b*-PS triblock copolymers are summarized in Figure 3D, and the linear increase in $M_{n,GPC}$ with the monomer conversion as well as the PDI values below 1.3 is indicated. The PNIPAM-*b*-PDMAEMA-*b*-PS triblock copolymers are also characterized by ^1H NMR analysis, and Figure 2C shows the spectra of the typical PNIPAM$_{54}$-*b*-PDMAEMA$_{27}$-*b*-PS$_{406}$ triblock copolymer. The $M_{n,NMR}$ of the PNIPAM-*b*-PDMAEMA-*b*-PS triblock copolymer is calculated by comparing the proton resonance signals at δ = 6.26 ~ 7.22 and 3.88 ~ 4.22 ppm. It is found that $M_{n,NMR}$ of the triblock copolymer is larger than $M_{n,GPC}$ by GPC analysis (Figure 3D), and the reason is due to the interaction between the tertiary amine groups in the PDMAEMA block and the GPC columns as discussed above.

The PNIPAM-*b*-PDMAEMA-*b*-PS triblock copolymer as well as the reference polymers is also characterized by DSC analysis (Figure S3), and three glass transition temperatures corresponding to the PDMAEMA block, the PS block, and the PNIPAM block are observed, suggesting that the three blocks of PDMAEMA, PS, and PNIPAM are immiscible.
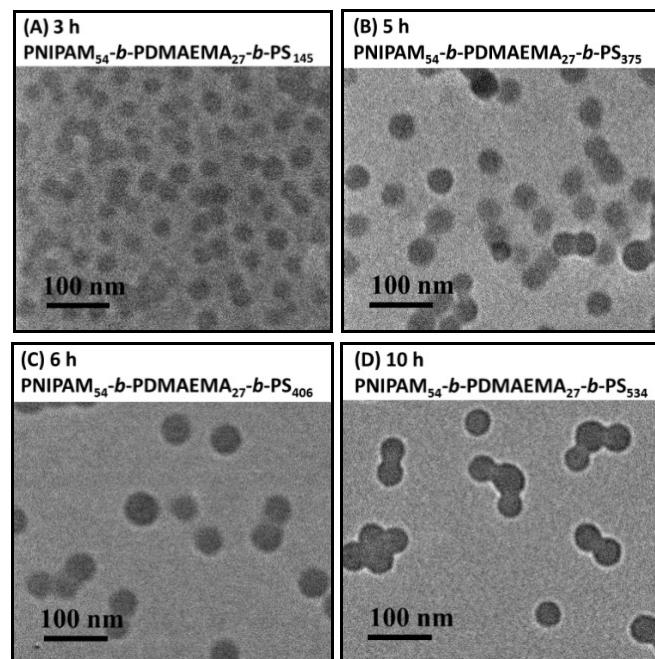

Scheme 3. The dispersion RAFT polymerization of styrene in the presence of PNIPAM$_{54}$-*b*-PDMAEMA$_{27}$-TTC macro-RAFT agents.
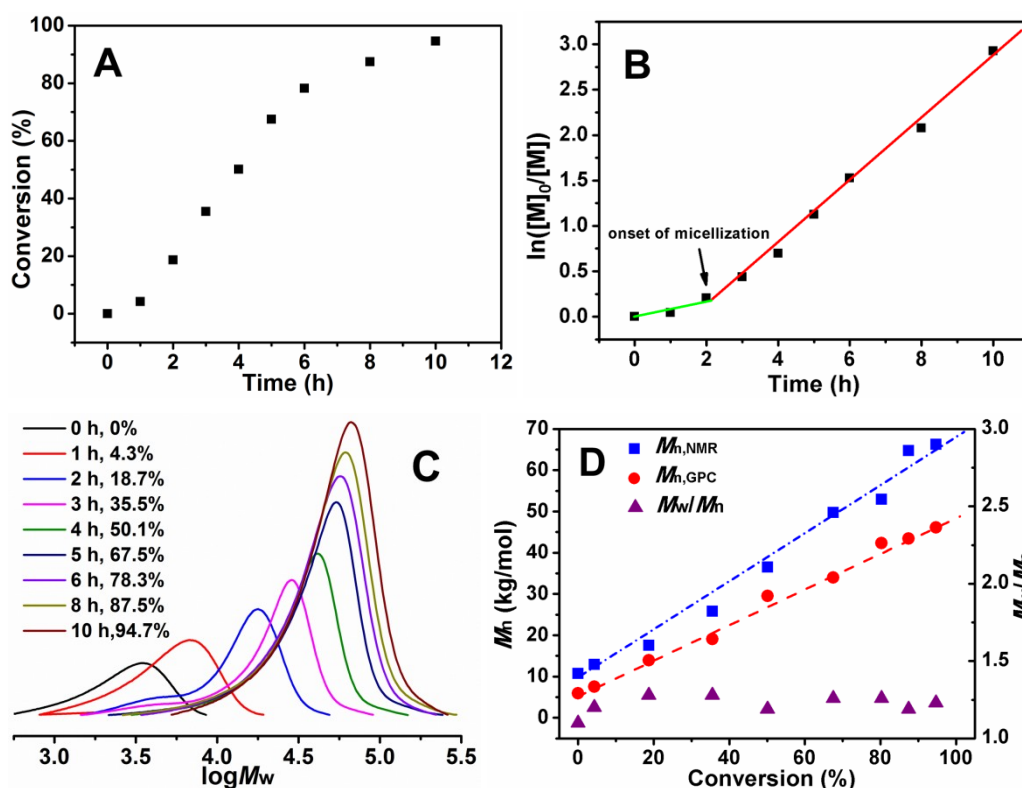
Figure 3. The monomer conversion-time plots (A) and the ln([M]$_0$/[M])-time plots (B) for the dispersion RAFT polymerization of styrene in the presence of PNIPAM$_{54}$-b-PDMAEMA$_{27}$-TTC; the GPC traces (C) and the evolution of the molecular weight and the PDI (M_n/M_w) value (D) of the synthesized PNIPAM-b-PDMAEMA-b-PS triblock copolymers.

The PNIPAM$_{54}$-b-PDMAEMA$_{27}$-TTC macro-RAFT agent mediated dispersion RAFT polymerization of styrene affords the in situ synthesis of the concentrated PNIPAM-b-PDMAEMA-b-PS triblock copolymer nanoparticles. These triblock copolymer nanoparticles are stably dispersed in the polymerization medium of the 80/20 methanol/water mixture. As indicated by the TEM images shown in Figures 4A-4D, uniform spherical nanoparticles are observed. The average diameter (D) of the triblock copolymer nanoparticles is evaluated by the statistical analysis of above 100 particles and the value is summarized in Figure 5, in which the increasing diameter D from 25 to 48 nm with the polymerization time is indicated. Compared with the PNIPAM$_{54}$-b-PDMAEMA$_{27}$-TTC macro-RAFT agent, PNIPAM$_{54}$-b-PDMAEMA$_{46}$-TTC and PNIPAM$_{54}$-b-PDMAEMA$_{58}$-TTC contain a PNIPAM block with the same DP but a little longer PDMAEMA block. Similarly, uniform 40 nm triblock copolymer nanoparticles of PNIPAM$_{54}$-b-PDMAEMA$_{46}$-b-PS$_{460}$ (Figure S4A) and 54 nm nanoparticles of PNIPAM$_{54}$-b-PDMAEMA$_{58}$-b-PS$_{546}$ (Figure S4B) are prepared through the dispersion RAFT polymerization by employing PNIPAM$_{54}$-b-PDMAEMA$_{46}$-TTC or PNIPAM$_{54}$-b-PDMAEMA$_{58}$-TTC as macro-RAFT agent. Since the PNIPAM and PDMAEMA blocks are soluble and the PS block is insoluble in the solvent of the 80/20 methanol/water mixture, these PNIPAM-b-PDMAEMA-b-PS triblock copolymer nanoparticles are expected to have corona-core structure, in which the soluble PNIPAM and PDMAEMA blocks form the

corona and the insoluble PS block forms the core as shown in Scheme 4A.

Figure 4. The TEM images of triblock copolymer nanoparticles of PNIPAM$_{54}$-b-PDMAEMA$_{27}$-b-PS$_{145}$ (A), PNIPAM$_{54}$-b-PDMAEMA$_{27}$-b-PS$_{375}$ (B), PNIPAM$_{54}$-b-PDMAEMA$_{27}$-b-PS$_{406}$ (C), and PNIPAM$_{54}$-b-PDMAEMA$_{27}$-b-PS$_{534}$ (D) prepared through the dispersion RAFT polymerization at different polymerization time.
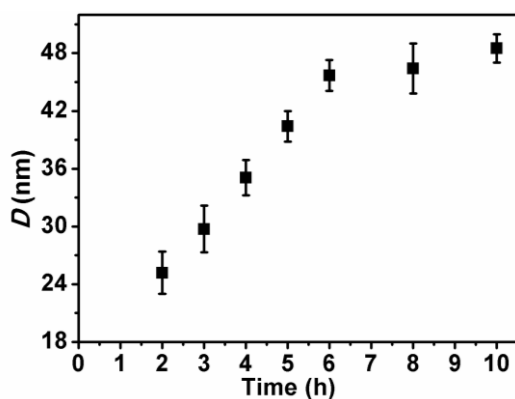
Figure 5. The average diameter D of the PNIPAM-*b*-PDMAEMA-*b*-PS triblock copolymer nanoparticles prepared through the dispersion RAFT polymerization.
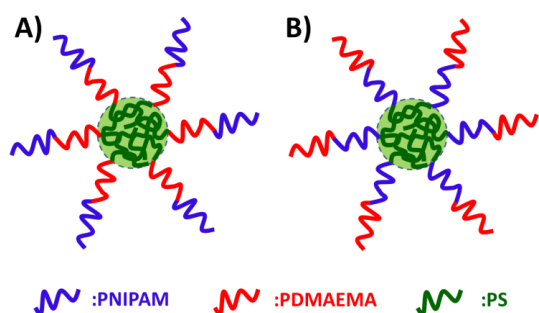
Scheme 4. The PNIPAM-*b*-PDMAEMA-*b*-PS (A) and PDMAEMA-*b*-PNIPAM-*b*-PS (B) triblock copolymer nanoparticles.

The PDMAEMA-*b*-PNIPAM-TTC macro-RAFT agent mediated dispersion polymerization of styrene is further checked, in which an initial homogeneous stage and a subsequent heterogeneous one are also optically observed similarly with the case of the PNIPAM-*b*-PDMAEMA-TTC macro-RAFT agent. Figure S5 shows the TEM images of two typical triblock copolymer nanoparticles of PDMAEMA$_{30}$-*b*-PNIPAM$_{68}$-*b*-PS$_{482}$ (D = 49 nm) and PDMAEMA$_{30}$-*b*-PNIPAM$_{106}$-*b*-PS$_{435}$ (D = 46 nm) at almost complete monomer conversion. The PDMAEMA-*b*-PNIPAM-*b*-PS triblock copolymers are characterized by ^{1}H NMR analysis (Figure S1), GPC analysis (Figure S2), and DSC analysis (Figure S6), respectively. The PDMAEMA-*b*-PNIPAM-*b*-PS triblock copolymer nanoparticles are expected to have corona-core structure as shown in Scheme 4B similar with the PNIPAM-*b*-PDMAEMA-*b*-PS nanoparticles except the different block order in the corona-forming blocks.

The triblock copolymer nanoparticles dispersed in water are characterized by DLS analysis, in which the narrowly distributed hydrodynamic diameter D_h are detected (Figure S9). The D_h of the triblock copolymer nanoparticles by DLS analysis is larger than that by TEM observation. Two reasons are ascribed to the difference between the DLS analysis and the TEM observation. First, the TEM observation shows the dried aggregates or the core of the triblock copolymer nanoparticles, while DLS analysis detects the solvated nanoparticles. Second, the DLS analysis shows an intensity-weighted diameter, while the TEM observation shows a number-average diameter, and the former is always oversized to the latter.

3.4 Double thermo-response of the triblock copolymer nanoparticles

The PNIPAM-*b*-PDMAEMA-*b*-PS and PDMAEMA-*b*-PNIPAM-*b*-PS triblock copolymers contain two thermo-responsive blocks of PNIPAM and PDMAEMA, and therefore their double temperature-sensitive response is expected. To check the thermo-response of the triblock copolymer nanoparticles, these triblock copolymer nanoparticles prepared through the dispersion RAFT polymerization in the 80/20 methanol/water mixture are transferred into water by dialysis against water at room temperature for three days (molecular weight cutoff: 7000 Da), and diluted with water to 0.2 wt% polymer concentration, and then the transmittance of the aqueous dispersion of the triblock copolymer nanoparticles at a given temperature is checked. Clearly, this transfer of the triblock copolymer nanoparticles from the 80/20 methanol/water mixture into water does not change the morphology of the triblock copolymer nanoparticles, since these triblock copolymer nanoparticles are frozen in the solvent of the 80/20 methanol/water mixture or neat water at room temperature.
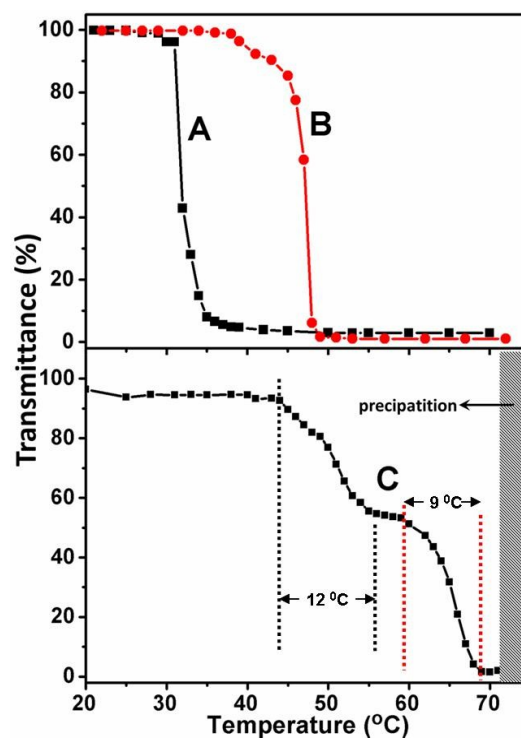
Figure 6. The transmittance *versus* temperature plots for the aqueous solution of the reference homopolymers of PNIPAM$_{54}$ (A) and PDMAEMA$_{30}$ (B), and the aqueous dispersion of the PNIPAM$_{54}$-*b*-PDMAEMA$_{46}$-*b*-PS$_{460}$ nanoparticles (C).

Figure 6 compares the thermo-response of the aqueous solutions of the reference homopolymers of PNIPAM$_{54}$ and PDMAEMA$_{30}$ (seeing the synthesis and characterization in Supporting Information) and the aqueous dispersion of the PNIPAM$_{54}$-*b*-PDMAEMA$_{46}$-*b*-PS$_{460}$ nanoparticles. As shown

in Figures 6A and 6B, high transmittance are observed at low temperature followed by a drastic decrease in the transmittance at 33 °C for the reference PNIPAM$_{54}$ homopolymer and at 47 °C for the reference PDMAEMA$_{30}$ homopolymer, respectively, indicating the sharp LCST-type phase transitions. The LCSTs of the present PNIPAM$_{54}$ and PDMAEMA$_{30}$ homopolymers match well with those reported elsewhere.[10-14] For the aqueous dispersion of the PNIPAM$_{54}$-*b*-PDMAEMA$_{46}$-*b*-PS$_{460}$ nanoparticles, two separate LCSTs are clearly observed. The transmittance starts to decrease at 44 °C with a middle point at 50 °C corresponding to the first LCST of the PNIPAM block, and it further decreases at 59 °C with a middle point at 67 °C corresponding to the second LCST of the PDMAEMA block. The further increase in temperature leads to precipitation of the triblock copolymer nanoparticles. Compared with the reference homopolymers of PNIPAM$_{54}$ (33 °C) and PDMAEMA$_{30}$ (47 °C), both the first LCST of the PNIPAM block (50 °C) and the second LCST of the PDMAEMA block (67 °C) tethered on the PS core of the triblock copolymer nanoparticles shift to high values. Besides, for the triblock copolymer nanoparticles, the thermo-responsive transition of the PNIPAM and PDMAEMA blocks takes place within a broad temperature range (12 °C for the PNIPAM block and 9 °C for the PDMAEMA block as indicated by the insets in Figure 6). The reason is possibly due to the steric repulsion among the crowded PNIPAM and PDMAEMA chains tethered on the PS core of the triblock copolymer nanoparticles (Note: the chain density of PNIPAM/PDMAEMA on the PS core of the triblock copolymer nanoparticles is about 0.055 nm^{-2} calculated by eq S3), which retards the soluble-to-insoluble transition of the tethered PNIPAM/PDMAEMA chains as discussed elsewhere.[66] Besides, there possibly exists strong interaction between the PNIPAM and PDMAEMA blocks through hydrogen bonding, which shifts the soluble-to-insoluble transition of the PNIPAM/PDMAEMA chains at high temperatures.
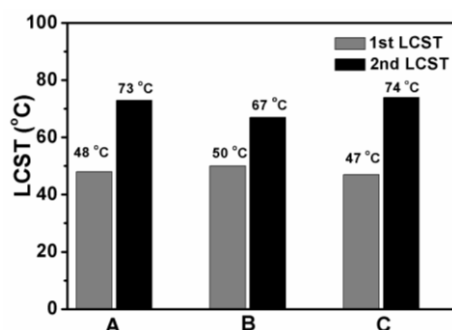

Figure 7. The LCST values of the aqueous dispersion of the triblock copolymer nanoparticles of PNIPAM$_{54}$-*b*-PDMAEMA$_{27}$-*b*-PS$_{519}$ (A), PNIPAM$_{54}$-*b*-PDMAEMA$_{46}$-*b*-PS$_{460}$ (B), and PNIPAM$_{54}$-*b*-PDMAEMA$_{58}$-*b*-PS$_{546}$ (C), in which the LCST values are determined at the middle point of the transmittance change.

The thermo-response of the aqueous dispersion of the PNIPAM$_{54}$-*b*-PDMAEMA$_{27}$-*b*-PS$_{519}$ and PNIPAM$_{54}$-*b*-PDMAEMA$_{58}$-*b*-PS$_{546}$ triblock copolymer nanoparticles is also checked, and two separate LCSTs corresponding to the PNIPAM and PDMAEMA blocks are also detected (Figure S7).

In these three triblock copolymer nanoparticles, the DP of the PNIPAM block keeps constant, and an almost constant LCST at 47-50 °C as shown in Figure 7 is detected. It was previously reported that the LCST of PDMAEMA was positively correlative to the polymer DP, that is, the LCST increased with the DP of PDMAEMA.[67] In the present study, the second LCST seems to be independent of the DP of the PDMAEMA block tethered on the core of the triblock copolymer nanoparticles, suggesting that the steric repulsion and the strong interaction between the PNIPAM and PDMAEMA blocks exceed the DP effect on the LCST of the PDMAEMA block.
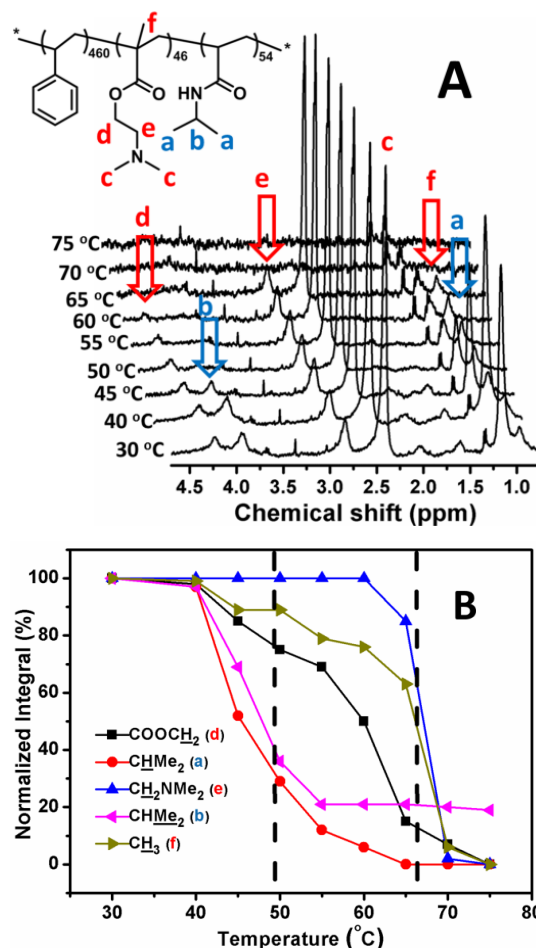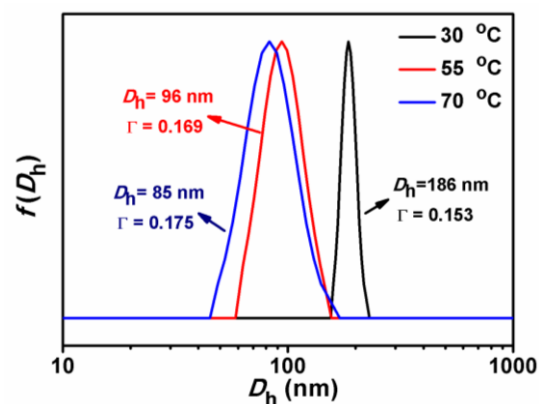

Figure 8. Temperature-dependent ^{1}H NMR spectra of the PNIPAM$_{54}$-*b*-PDMAEMA$_{46}$-*b*-PS$_{460}$ nanoparticles dispersed in D$_2$O (A) and the temperature-dependent normalized integrals of the five typical proton signals (B).

In order to gain close insight into the thermo-responsive behavior of the PNIPAM-*b*-PDMAEMA-*b*-PS nanoparticles, variable temperature ^{1}H NMR analysis of the typical PNIPAM$_{54}$-*b*-PDMAEMA$_{46}$-*b*-PS$_{460}$ nanoparticles dispersed in D$_2$O is made, and the ^{1}H NMR spectra are summarized in Figure 8A. At 30 °C, the proton signals assigned to the PNIPAM block [(**a**, CH(C**H$_3$**)$_2$) at δ = 1.17 ppm and (**b**, C**H**(CH$_3$)$_2$) at δ = 3.93 ppm] and the PDMAEMA block [(**c**, CH$_2$N(C**H$_3$**)$_2$] at δ = 2.38 ppm, (**d**, COOC**H$_2$**) at δ = 4.23 ppm, (**e**, C**H$_2$**N(CH$_3$)$_2$) at δ = 2.84 ppm, and (**f**, C**H$_3$**) at δ = 0.97 ppm]

are clearly discerned, and the area ratio of the peaks of (**b**, C*H*(CH$_3$)$_2$) and (**d**, COOC*H*$_2$) is very close to those recorded in CDCl$_3$, suggesting that both the PNIPAM and PDMAEMA blocks are soluble in D$_2$O at this temperature. Note: the PS block is insoluble in D$_2$O and very faint signal is detected, and therefore is not discussed herein. When temperature increases to 45 °C, the characteristic signals of the PDMAEMA block almost remain unchanged or slightly decrease compared with those at 30 and 40 °C, while the signals of (**b**, C*H*(CH$_3$)$_2$) and (**a**, CH(C*H*$_3$)$_2$) attributed to the PNIPAM block decrease much, indicating the beginning of the soluble-to-insoluble phase transition of the PNIPAM block. When the temperature increases to 50 °C above the first LCST of PNIPAM, the signals attributed to the PNIPAM block greatly decrease and become broaden, while the signals of the PDMAEMA block have no obvious change. Upon a further temperature increase to 55 °C, the signals attributed to the PNIPAM block are increasingly attenuated or disappeared, suggesting the dehydration of the PNIPAM block at temperature above the first LCST. When temperature increases to 65 °C, the PDMAEMA signals of (**d**, COOC*H*$_2$), (**e**, C*H*$_2$N(CH$_3$)$_2$) and (**f**, C*H*$_3$) start to decrease and become flattened when temperature further increases to 70 °C above the second LCST of the PDMAEMA block. To clarify the different thermo-response of the PNIPAM and PDMAEMA blocks with the increasing temperature, the typical proton signals of (**a**, CH(C*H*$_3$)$_2$) and (**b**, C*H*(CH$_3$)$_2$) attributed to the PNIPAM block and the signals of (**d**, COOC*H*$_2$), (**e**, C*H*$_2$NMe$_2$) and (**f**, C*H*$_3$) attributed to the PDMAEMA block are normalized to their values at 30 °C, and then the values are summarized in Figure 8B. As shown in Figure 8B, when temperature increases from 30 to 55 °C above the first LCST of the PNIPAM block, the signals of (**a**, CH(C*H*$_3$)$_2$) and (**b**, C*H*(CH$_3$)$_2$) attributed to the PNIPAM block decreases by about 88% and 79%, and the signals of (**d**, COOC*H*$_2$), (**e**, C*H*$_2$N(CH$_3$)$_2$) and (**f**, C*H*$_3$) attributed to the PDMAEMA keep constant or just slightly decrease by 31%, indicating the PNIPAM block undergoing the soluble-to-insoluble phase transition and the PDMAEMA block keeping soluble at this temperature. When temperature further increases from 55 to 70 °C above the second LCST of the PDMAEMA block, the signals of (**d**, COOC*H*$_2$), (**e**, C*H*$_2$N(CH$_3$)$_2$) and (**f**, C*H*$_3$) sharply decreases by 62%, 98% and 73%, respectively, suggesting the dehydration of the PDMAEMA block at this temperature. Besides, the decrease in the signal of (**a**, CH(C*H*$_3$)$_2$) attributed to the PNIPAM block and those of (**d**, COOC*H*$_2$) and (**f**, C*H*$_3$) attributed to the PDMAEMA block occurs at a wide temperature range crossing from the first LCST to above the second LCST, which suggests the soluble-to-insoluble phase transition occurring within a wide temperature range as shown in Figure 6C.

The thermo-responsive behavior of the PNIPAM$_{54}$-*b*-PDMAEMA$_{46}$-*b*-PS$_{460}$ triblock copolymer nanoparticles dispersed in water was further confirmed by DLS analysis.

Before DLS analysis, these triblock copolymer nanoparticles were diluted with water to 0.02 wt% polymer concentration to avoid inter-nanoparticle aggregation or formation of nanoparticle-clusters when temperature increases above LCST of the thermo-responsive blocks. The TEM images of the diluted aqueous dispersion of the triblock copolymer nanoparticles at 30, 45 and 70 °C are shown in Figure S8, in which uniform 40 nm nanoparticles are detected at three cases of temperature, confirming no disassembly or inter-nanoparticle aggregation during the heating of the diluted dispersion of the triblock copolymer nanoparticles. Figure 9 shows the hydrodynamic diameter (D_h) of the PNIPAM$_{54}$-*b*-PDMAEMA$_{46}$-*b*-PS$_{460}$ nanoparticles at temperature of 30 °C below the first LCST, at 55 °C above the first LCST, and at 70 °C above the second LCST, respectively. DLS analysis of the aqueous dispersion of the triblock copolymer nanoparticles at temperature higher than 70 °C is not made, since precipitation of these triblock copolymer nanoparticles occurs. As shown in Figure 9, the hydrodynamic diameter distribution $f(D_h)$ of the triblock copolymer nanoparticles is narrowly dispersed and the hydrodynamic diameter D_h decreases when temperature increases above the first LCST of the PNIPAM block and D_h further decreases at temperature above the second LCST of the PDMAEMA block, confirming the two-step shrinkage of the PNIPAM$_{54}$-*b*-PDMAEMA$_{46}$-*b*-PS$_{460}$ nanoparticles upon temperature increasing as shown in Scheme 5. That is, when temperature increases above the first LCST of the PNIPAM block, the outer PNIPAM block becomes dehydrated and deposited onto the PS core to form corona-shell-core nanoparticles, in which the solvophobic PS block forms the core, the dehydrated PNIPAM forms the shell and the looped PDMAEMA block forms the corona; when temperature increases above the second LCST of the PDMAEMA block, the PDMAEMA block dehydrates to form shell-shell-core structure; when temperature further increases, aggregation of the triblock copolymer shell-shell-core nanoparticles occurs.


Figure 9. Hydrodynamic diameter distribution $f(D_h)$ of the PNIPAM$_{54}$-*b*-PDMAEMA$_{46}$-*b*-PS$_{460}$ nanoparticles dispersed in water at 30 °C, 55 °C, and 70 °C.
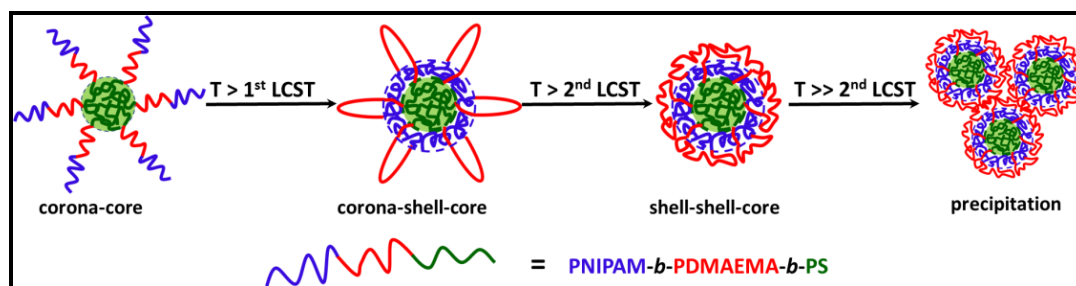
Scheme 5. Schematic illustration of the doubly thermo-responsive behavior of the PNIPAM-*b*-PDMAEMA-*b*-PS nanoparticles dispersed in water upon temperature increasing.

The thermo-response of the PDMAEMA$_{30}$-*b*-PNIPAM$_{68}$-*b*-PS$_{482}$ nanoparticles dispersed in water is also checked. As shown in Figure 10, two separate LCSTs are discerned in the temperature dependent transmittance of the aqueous dispersion of the PDMAEMA$_{30}$-*b*-PNIPAM$_{68}$-*b*-PS$_{482}$ nanoparticles similarly with those of the PNIPAM$_{54}$-*b*-PDMAEMA$_{46}$-*b*-PS$_{460}$ nanoparticles, although the two triblock copolymers have different block order. In comparison, the first LCST corresponding to the PNIPAM block, 43 $^{\circ}$C, and the second LCST corresponding to the PDMAEMA block, 63 $^{\circ}$C, in the PDMAEMA$_{30}$-*b*-PNIPAM$_{68}$-*b*-PS$_{482}$ nanoparticles are lower than those in the PNIPAM$_{54}$-*b*-PDMAEMA$_{46}$-*b*-PS$_{460}$ nanoparticles. It is expected that, the different block order of the PNIPAM and PDMAEMA blocks leads to different steric repulsion among the crowded PNIPAM and PDMAEMA chains tethered on the PS core of the triblock copolymer nanoparticles, and therefore leads to different LCSTs of the thermo-responsive blocks. Furthermore, the transmittance of the aqueous dispersion of the PDMAEMA$_{30}$-*b*-PNIPAM$_{68}$-*b*-PS$_{482}$ nanoparticles just decreases by 3.5% upon temperature increasing above the second LCST of the PDMAEMA block, which is much feeble than that of the PNIPAM$_{54}$-*b*-PDMAEMA$_{46}$-*b*-PS$_{460}$ nanoparticles shown in Figure 6, suggesting the great difference in the thermo-response of the PDMAEMA$_{30}$-*b*-PNIPAM$_{68}$-*b*-PS$_{482}$ and PNIPAM$_{54}$-*b*-PDMAEMA$_{46}$-*b*-PS$_{460}$ nanoparticles, although the exact reason needs further study.
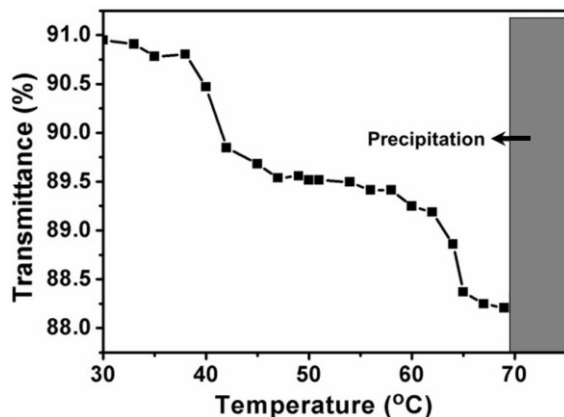
Figure 10 Transmittance *versus* temperature plots for the aqueous dispersion of the PDMAEMA$_{30}$-*b*-PNIPAM$_{68}$-*b*-PS$_{482}$ nanoparticles.

4 Conclusions

Doubly thermo-responsive triblock copolymer nanoparticles of PNIPAM-*b*-PDMAEMA-*b*-PS and PDMAEMA-*b*-PNIPAM-*b*-PS containing a PS core and a corona of two thermo-responsive PNIPAM and PDMAEMA blocks are prepared through macro-RAFT agent mediated dispersion polymerization of styrene in the 80/20 methanol/water mixture by employing the diblock copolymer macro-RAFT agent of PNIPAM-*b*-PDMAEMA-TTC or PDMAEMA-*b*-PNIPAM-TTC. The dispersion RAFT polymerization initially undergoes a slow homogeneous polymerization and then a fast heterogeneous polymerization follows. During the dispersion RAFT polymerization, the molecular weight of the synthesized triblock copolymer linearly increases with the monomer conversion till to almost complete monomer conversion, and the average diameter determined by TEM of the in situ synthesized triblock copolymer nanoparticles increases with the triblock copolymer molecular weight. The PNIPAM-*b*-PDMAEMA-*b*-PS and PDMAEMA-*b*-PNIPAM-*b*-PS nanoparticles dispersed in water exhibit two separate LCSTs corresponding to the PNIPAM block and the PDMAEMA block, and this two-step thermo-responsive behavior is evidenced by the combined techniques including turbidity analysis, variable temperature ^{1}H NMR analysis, DLS analysis and TEM observation. For the PNIPAM-*b*-PDMAEMA-*b*-PS nanoparticles dispersed in water, the first LCST corresponding to the PNIPAM block and the second LCST corresponding to the PDMAEMA block are higher than those of the reference homopolymers, and the reason is ascribed to the steric repulsion and the strong interaction between the PNIPAM and PDMAEMA blocks tethered on the PS core of the triblock copolymer nanoparticles. Upon temperature increasing above the first LCST, the PNIPAM block becomes dehydrated to deposit on the PS core, and the PNIPAM-*b*-PDMAEMA-*b*-PS corona-core nanoparticles convert into corona-shell-core ones; when temperature further increasing above the second LCST, the PDMAEMA chains becomes dehydrated to form shell-shell-core nanoparticles.

Acknowledgements

Polymer Chemistry Accepted Manuscript

Notes and references

1   D. Roy, W. L. A. Brooks, B. S. Sumerlin, *Chem. Soc. Rev.* **2013,** 42, 7214-7243.

2   V. Aseyev, H. Tenhu, F. M. Winnik, *Adv. Polym. Sci.* **2011**, 242, 29-89.

3   Y. Zhu, J. Y. Quek, A. B. Lowe, P. J. Roth, *Macromolecules* **2013,** 46, 6475-6484.

4   J. M. Bak, K.-B. Kim, J.-E. Lee, Y. Park, S. S. Yoon, H. M. Jeong, H.-I. Lee, *Polym. Chem.* **2013,** 4, 2219-2223.

5   S. Monge, S. Antoniacomi, V. Lapinte, V. Darcos, J.-J Robin, *Polym. Chem.* **2012,** 3, 2502-2507.

6   G. B. H. Chua, Peter. J. Roth, H. T. T. Duong, T. P. Davis, A. B. Lowe, *Macromolecules* **2012,** 45, 1362-1374.

7   Y. Zou, D. E. Brooks, J. N. Kizhakkedathu, *Macromolecules* **2008**, 41, 5393-5405.

8   D. J. Phillips, M. I. Gibson, *Chem. Commun.* **2012,** 48, 1054-1056.

9   C.-T Lai, R.-H. Chien, S.-W. Kuo, J.-L. Hong, *Macromolecules* **2011,** 44, 6546-6556.

10 M. E. Alf, T. A. Hatton, K. K. Gleason, *Polymer* **2011,** 52, 4429-4434.

11 J. Xu, J. Ye, S. Liu, *Macromolecules* **2007,** 40, 9103-9110.

12 R. Plummer, D. J. T. Hill, A. K. Whittaker, *Macromolecules* **2006,** 39, 8379-8388.

13 D. Fournier, R. Hoogenboom, H. M. L. Thijs, R. M. Paulus, U. S. Schubert, *Macromolecules* **2007,** 40, 915-920.

14 F. A. Plamper, M. Ruppel, A. Schmalz, O. Borisov, M. Ballauff, A. H. E. Mü1ller, *Macromolecules* **2007,** 40, 8361-8366.

15 S. Glatzel, A. Laschewsky, J.-F. Lutz, *Macromolecules* **2011,** 44, 413-415.

16 C. Pietsch, R. Hoogenboom, U. S. Schubert, *Polym. Chem.* **2010,** 1, 1005-1008.

17 Q. Zhang, P. Schattling, P. Theato, R. Hoogenboom, *Polym. Chem.* **2012,** 3, 1418-1426.

18 T. Ueki, Y. Nakamura, A. Yamaguchi, K. Niitsuma, T. P. Lodge, M. Watanabe, *Macromolecules* **2011,** 44, 6908-6914.

19 G. V. Assche, B. V. Mele, T. Li, E. Nies, *Macromolecules* **2011,** 44, 993-998.

20 C. Li, N. J. Buurma, I. Haq, C. Turner, S. P. Armes, *Langmuir* **2005,** 21, 11026-11033.

21 F. D. Jochum, P. J. Roth, D. Kessler, P. Theato, *Biomacromolecules* **2010,** 11, 2432-2439.

22 J. Weiss, A. Laschewsky, *Macromolecules* **2012,** 45, 4158-4165.

23 H. Wei, S. Perrier, S. Dehn, R. Ravarian, F. Dehghani, *Soft Matter* **2012,** 8, 9526-9528.

24 C. Pietsch, U. Mansfeld, C. Guerrero-Sanchez, S. Hoeppener, A. Vollrath, M. Wagner, R. Hoogenboom, S. Saubern, S. H. Thang, C. R. Becer, J. Chiefari, U. S. Schubert, *Macromolecules* **2012,** 45, 9292-9302.

25 P. J. Roth, T. P. Davis, A. B. Lowe, *Macromolecules* **2012,** 45, 3221-3230.

26 H.-N. Lee, Z. Bai, N. Newell, T. P. Lodge, *Macromolecules* **2010,** 43, 9522-9528.

27 Y. Su, M. Dan, X. Xiao, X. Wang, W. Zhang, *J. Polym. Sci. Part A: Polym. Chem.* **2013,** 51, 4399-4412.

28 M. Dan, Y. Su, X. Xiao, S. Li, W. Zhang, *Macromolecules* **2013,** 46, 3137-3146.

29 C. Mu, X. Fan, W. Tian, Y. Bai, X. Zhou, *Polym. Chem.* **2012,** 3, 1137-1149.

30 X. J. Loh, Z.-X. Zhang, Y.-L. Wu, T. S. Lee, J. Li, *Macromolecules* **2009,** 42, 194-202.

31 X. Liu, P. Ni, J. He, M. Zhang, *Macromolecules* **2010,** 43, 4771-4781.

32 B. H. Lessard, E. J. Y. Ling, M. Marić, *Macromolecules* **2012,** 45, 1879-1891.

33 J. Weiss, A. Li, E. Wischerhoff, A. Laschewsky, *Polym. Chem.* **2012,** 3, 352-361.

34 M. E. Levere, H. T. Ho, S. Pascual, L. Fontaine, *Polym. Chem.* **2011,** 2, 2878-2887.

35 C. Zhou, M. A. Hillmyer, T. P. Lodge, *Macromolecules* **2011,** 44, 1635-1641.

36 X. Xu, J. D. Flores, C. L. McCormick, *Macromolecules* **2011,** 44, 1327-1334.

37 Y. Li, B. S. Lokitz, C. L. McCormick, *Macromolecules* **2006,** 39, 81-89.

38 B. Charleux, G. Delaittre, J. Rieger, F. D'Agosto, *Macromolecules* **2012,** 45, 6753-6765.

39 J.-T. Sun, C.-Y. Hong. C.-Y. Pan, *Polym. Chem.* **2013,** 4, 873-881.

40 I. Chaduc, A. Crepet, O. Boyron, B. Charleux, F. D'Agosto, M. Lansalot, *Macromolecules* **2013,** 46, 6013-6023.

41 W. Zhang, F. D'Agosto, P.-Y. Dugas, J. Rieger, B. Charleux, *Polymer* **2013,** 54, 2011-2019.

42 W.-M. Wan, C.-Y. Pan, *Macromolecules* **2010,** 43, 2672-2675.

43 W. Shen, Y. Chang, G. Liu, H. Wang, A. Cao, Z. An, *Macromolecules* **2011,** 44, 2524-2530.

44 W. Zhang, F. D'Agosto, O. Boyron, J. Rieger, B. Charleux, *Macromolecules* **2012,** 45, 4075-4084.

45 C. N. Urbani, M. J. Monteiro, *Macromolecules* **2009,** 42, 3884-3886.

46 N. Chan, M. F. Cunningham, R. A. Hutchinson, *Polym. Chem.* **2012,** 3, 486-497.

47 C. J. Ferguson, R. J. Hughes, D. Nguyen, B. T. T. Pham, R. G. Gilbert, A. K. Serelis, C. H. Such, B. S. Hawkett, *Macromolecules* **2005,** 38, 2191-2204.

48 J. Rosselgong, A. Blanazs, P. Chambon, M. Williams, M. Semsarilar, J. Madsen, G. Battaglia, S. P. Armes, *ACS Macro Lett.* **2012,** 1, 1041-1045.

49 M. Semsarilar, V. Ladmiral, A. Blanazs, S. P. Armes, *Langmuir* **2013,** 29, 7416-7424.

50 A. Blanazs, A. J. Ryan, S. P. Armes, *Macromolecules* **2012,** 45, 5099-5107.

51 D. Zehm, L. P. D. Ratcliffe, S. P. Armes, *Macromolecules* **2013,** 46, 128-139.

Polymer Chemistry Accepted Manuscript

52 M. Semsarilar, V. Ladmiral, A. Blanazs, S. P. Armes, *Langmuir* **2012,** 28, 914-922.

53 A. Blanazs, J. Madsen, G. Battaglia, A. J. Ryan, S. P. Armes, *J. Am. Chem. Soc.* **2011,** 133, 16581-16587.

54 Y. Su, X. Xiao, S. Li, M. Dan, X. Wan, W. Zhang, *Polym. Chem.* **2014**, 5, 578-587.

55 M. Dan, F. Huo, X. Zhang, X. Wang, W. Zhang, *J. Polym. Sci. Part A: Polym. Chem.* **2013,** 51, 1573-1584.

56 X. Wang, S. Li, Y. Su, F. Huo, W. Zhang, *J. Polym. Sci. Part A: Polym. Chem.* **2013,** 51, 2188-2198.

57 J. Xu, X. Xiao, Y. Zhang, W. Zhang, P. Sun, *J. Polym. Sci. Part A: Polym. Chem.* **2013,** 51, 1147-1161.

58 X. Xiao, S. He, M. Dan, Y. Su, F. Huo, W. Zhang, *J. Polym. Sci. Part A: Polym. Chem.* **2013,** 51, 3177-3190.

59 X. Wang, J. Xu, Y. Zhang, W. Zhang, *J. Polym. Sci. Part A: Polym. Chem.* **2012,** 50, 2452-2462.

60 Z. An, Q. Shi, W. Tang, C.-K. Tsung, C. J. Hawker, G. D. Stucky, *J. Am. Chem. Soc.* **2007,** 129, 14493-14499.

61 G. Moad, Y. K. Chong, A. Postma, E. Rizzardo, S. H. Thang, *Polymer* **2005,** 46, 8458-8468.

62 H. de Brouwer, M. A. J. Schellekens, B. Klumperman, M. J. Monteiro, A. L. German, *J. Polym. Sci. Part A: Polym. Chem.* **38,** 3596-3603.

63 A. P. Narrainen, A. Pascual, D. M. Haddleton, *J. Polym. Sci. Part A: Polym. Chem.***2002,** 40, 439-450.

64 C. Schilli, M. G. Lanzendörfer, A. H. E. Müller, *Macromolecules* **2002,** 35, 6819-6827.

65 M. J. Monteiro and J. de Barbeyrac, *Macromolecules* **2001,** 34, 4416-4423.

66 C. Yang, J. N. Kizhakkedathu, D. E. Brooks, F. Jin, C. Wu, *J. Phys. Chem. B* **2004,** 108, 18479-18484.

67 X. Han, X. Zhang, H. Zhu, Q. Yin, H. Liu, Y. Hu, *Langmuir* **2013,** 29, 1024-1034.

Polymer Chemistry Accepted Manuscript